# Impact demagnetization of the Martian crust: Primaries versus secondaries

N. Artemieva,[1] L. Hood,[2] and B. A. Ivanov[1]

Received 12 August 2005; revised 19 October 2005; accepted 21 October 2005; published 30 November 2005.

[1] Numerical simulations presented here show that demagnetization of crust near the largest Martian basins by secondary impacts can be comparable to that by direct shock waves outside the transient cavity. The relative input from secondary impacts, which demagnetize only the uppermost layers, depends on the magnetic carrier distribution within the crust. Thus, we discuss properties of likely magnetic remanence carriers and their possible spatial distribution within the crust. **Citation:** Artemieva, N., L. Hood, and B. A. Ivanov (2005), Impact demagnetization of the Martian crust: Primaries versus secondaries, *Geophys. Res. Lett.*, *32*, L22204, doi:10.1029/2005GL024385.

## 1. Introduction

[2] The lack of magnetic anomalies within the giant Martian impact basins, Hellas, Argyre, and Isidis is well established on the basis of the Mars Global Surveyor magnetometer data [*Acuña et al.*, 1999] and the role of impact demagnetization by direct shock waves has been estimated analytically [*Hood et al.*, 2003; *Mohit and Arkani-Hamed*, 2004]. In this paper we present numerical calculations of the shock wave decay in giant impacts, corresponding to the known Martian basins and compare inputs from direct basin-forming impacts and secondary impacts by high-velocity ejecta from these basins.

## 2. Numerical Models

[3] To model formation of a large basin after a vertical impact as well as smaller and lower velocity (1–5 km/s) secondary craters we use the two-dimensional SALEB code, originally described by *Amsden et al.* [1980] and recently modified by *Ivanov* [2003]. The early stage of an oblique impact (until transient cavity formation) is modeled with the three-dimensional code SOVA [*Shuvalov*, 1999] with simplified description of strength. Both codes are coupled with the ANEOS equation of state [*Thompson and Lauson*, 1972]. While shock wave decay in the target does not depend on the impact obliquity, deposition of high-velocity ejecta, responsible for secondary craters, differs substantially from a vertical impact. We use ballistic continuation for high-velocity (>1 km/s) ejecta to find the distribution of secondary craters and to estimate demagnetization caused by these impacts. For an independent rough estimate of the amount of secondary impacts, we also use the analytical Z-model [*Maxwell*, 1977] with a fragment size distribution derived from observations [*Moore*, 1971].

## 3. Target and Projectile Properties

[4] Although it is more accurate to model the largest basins, whose diameters are comparable to the planetary size, on a spherical target with self-gravity, as a first approximation, we consider here a planar constant-gravity target, consisting of two layers, a 50-km-thick crust (basalt equation of state) and an infinite mantle (dunite). The temperature gradient (16 K/km in the crust, 5 K/km in the upper 150 km of the mantle, and 0.2 K/km below) is consistent with recent estimates for ancient Mars [*Nimmo and Gilmore*, 2001; *Hauck and Phillips*, 2002].

[5] It is a non-trivial task to define the transient cavity diameter for known multi-ring basins. The problem has been discussed by *Hood et al.* [2003] and by *Mohit and Arkani-Hamed* [2004]. In the analytical estimates we use transient cavity sizes from 650 km to 1400 km, i.e. comprising all three Martian basins: Hellas (1300–1400 km), Isidis (900–1000 km), and Argyre (750–800 km). In the numerical models, the impact velocity varies from 8 to10 km/s according to modern average asteroid impact velocity on Mars [*Steel*, 1998]; a projectile diameter is in the range 150–600 km according to scaling laws [*Schmidt and Housen*, 1987]. However, scaling itself is not quite reliable for multi-ring basins. Moreover, during the modeling, it is very difficult to define the size of the resulting transient cavity because the crater modification (i.e., gravitational collapse) starts before the excavation, which defines the transient cavity size, is halted. The size of the final crater is also not very useful, as its morphological features, i.e. depth and ring diameters, are badly resolved even in two-dimensional simulations with 15 km resolution. Our impression, however, is that the largest projectile considered here of 600 km diameter is a bit larger than the actual Hellas projectile with the calculated transient cavity size, $D_{tr}$, after 45-degree impact of about 1800 km, while the smallest of 150 km diameter is a bit smaller than the Argyre projectile (calculated $D_{tr} \approx 600$ km after a 30-degree impact).

## 4. Demagnetization by the Direct Shock Wave

[6] The results of giant impact numerical simulations are shown in Figure 1. A 300-km-diameter projectile strikes vertically at 8 km/s. The transient cavity diameter is ~1000 km (probably comparable to that of the Isidis basin). In Figure 1 (top) the maximum shock compression is shown for the vertical tracers (solid lines with small symbols) and for the near-surface tracers (at a depth of 1–8 km). It is obvious that the shock pressure decays quickly near the free

[1]Institute for Dynamics of Geospheres, Moscow, Russia.
[2]Lunar and Planetary Laboratory, University of Arizona, Tucson, Arizona, USA.


0094-8276/05/2005GL024385

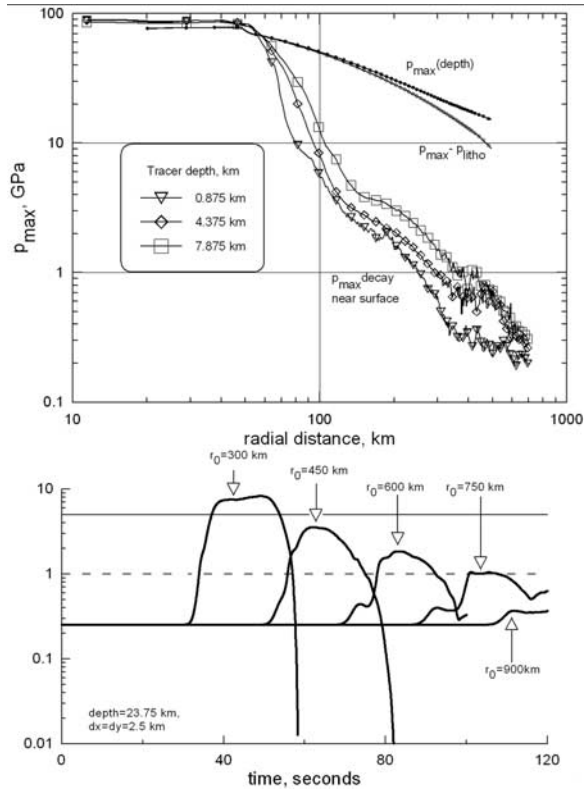


**Figure 1.** (top) Pressure decay vs distance from the impact point: under the projectile center (upper curves) and along the surface at selected depths (see text on the figure). 300-km-diameter asteroid strikes vertically at 8 km/s. (bottom) Pressure vs time in several mid-crust points for the same asteroid impact as in Figure 1 (top).

surface: at a radial distance of 300 km, it is ten times lower than in the vertical direction. Figure 1 (bottom) shows the shape of the pressure pulses in the middle of the crust (assumed thickness 50 km) at different distances from the impact point, from 2 to 6 projectile radius. The maximum shock compression is the result of at least 3 following shock waves (the first two definitely have been refracted and reflected from the mantle). The total maximum compression in the shock wave (sum of the initial lithostatic pressure of ~0.25 GPa plus shock overpressure) drops below 1 GPa in the middle of the crust at the distance of 750 km (~5 projectile radii).

[7] Adopting a reasonable threshold of ~1 GPa (horizontal dashed line in Figure 1, bottom) as a minimum pressure required for demagnetization, the results of our numerical modeling confirm analytic estimates by *Mohit and Arkani-Hamed* [2004]: direct shock waves can be responsible for crustal demagnetization only within the transient cavity. To investigate possible substantial demagnetization at larger distances, we study further secondary impacts (SI).

## 5. Demagnetization by Low-Velocity Secondary Impacts

[8] All fragments ejected with velocity below escape (5 km/s) strike the surface at some distance from the primary crater, creating secondary craters, boulders on the surface, or dusty ejecta blankets, depending on the fragment size and velocity. Secondary impacts may cause partial shock demagnetization of the upper crust. Based on the numerical modeling results, we calculate the ratio of a target volume $V_t$ compressed above 1 GPa to a projectile volume $V_{pr}$ for impacts with velocity $U$ ranging from 1 to 5 km/s. This ratio may be approximated as follows: $V_t/V_{pr} = 0.55U^{3.66}$, where $U$ is in km/s.

[9] To estimate the thickness of the crust demagnetized by secondary impacts we should also define their total amount and distribution around the basins. For this purpose, first, we use the simple Z-model and then compare the results with more accurate numerical simulations.

[10] *Z-model* [*Maxwell*, 1977] gives a power law decay of ejection velocity with distance from an impact point under the assumption of gravity-dominated crater [*Ivanov and Comissarova*, 1977]. The model also allows estimating the volume of material ejected with a given velocity. This volume may be treated as a single "fragment" or as separated fragments with a power size–frequency distribution calibrated with the largest fragments observed near the lunar craters [*Moore*, 1971; *Vickery*, 1986]. The results for the first case ("single fragment") are shown in Figure 2 by the lines with filled symbols for 3 values of $D_{tr}$. The effect strongly depends on the transient cavity size: while transient cavities for Hellas and Argyre differ by less than a factor of two (1400 km versus 800 km), the thickness of demagnetization near Hellas' transient cavity edge is 5 times larger (50 km and 10 km, respectively) with the former value close to the crust thickness). For the case with fragments, extrapolation of observations [*Moore*, 1971; *Artemieva and Ivanov*, 2004] to larger basins is not reliable, as crater diameter itself is poorly defined and the size of the largest block may be restricted by the crust structure (faulting, nonhomogeneity, etc.). However, we assume that demagnetization in a given point is due to the largest fragments striking this area. Smaller fragments lead to additional demagnetization, if they strike non-demagnetized area. The results are shown in Figure 2 by lines with open symbols. In this case demagnetization is substantially weaker – only the upper-

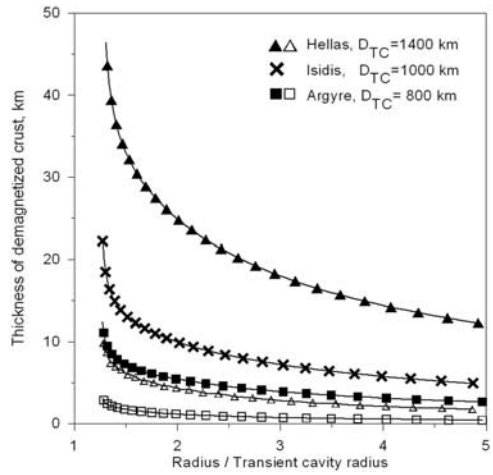


**Figure 2.** Demagnetization by secondary impacts for 3 TC diameters. Lines with filled symbols represent maximum estimates, with open symbols – more reliable estimates, which take secondary fragments SFD into account (see text for details).

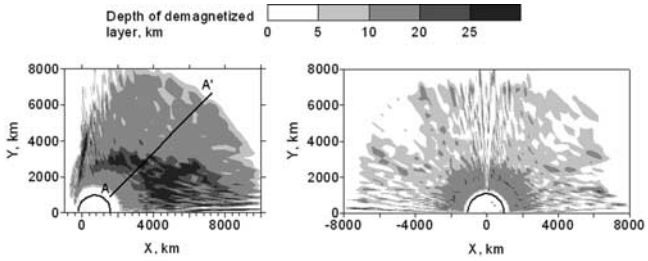


**Figure 3.** View from the sky at the impact basin (thick black line, ~1800 km). Thickness of the crust compressed above 1 GPa by secondary impacts as a function of distance from the impact point after a vertical impact (right) and a 45° impact (left). In the oblique impact X-axis is along the trajectory, the projectile comes from the left; Y is across the trajectory. Half-space (Y > 0) is shown.

most 12 km of the crust are demagnetized for the largest basin, and 2 km – for the smallest one. This estimate gives a lower limit of demagnetization by secondary impacts.

[11] The real situation, most probably, is a combination of both estimates: in the far zone separated fragments create well-separated secondary craters and demagnetize a thin upper layer of the crust (i.e. the lower limit gives correct answer); near the crater rim tight clusters (with density close to density of non-disrupted target material) operate as a single solid impactor.

[12] 3D numerical modeling of 600-km-diameter projectile impact allows us to calculate directly a total amount of high-velocity ejecta, its velocity and spatial distribution, and hence – distribution of secondary craters on the surface. Figure 3 shows the thickness of demagnetized crust in the case of a vertical impact (right) and a 45° impact (left). In the latter case the thickness of demagnetized crust is substantially asymmetric and stronger (up to 40 km) in the downrange direction. Figure 4 shows the thickness of demagnetization along the A-A' line: an input from every secondary impact along this line is shown by dots, while the solid line represents an average thickness over a square of 300 km × 300 km. Although individual impacts are more effective at large distances (higher impact velocity), their amount sharply decreases with distance and in average, demagnetization has maximum at 3000–4000 km from the crater center. In agreement with advanced Z–model (lines with open symbols in Figure 2) demagnetization is rather weak, 10–20 km, near the transient cavity. An interesting fact (and substantial disagreement with Z-model) is that there is no demagnetization close to the transient cavity edge. According to the numerical model, ejecta deposited here have a rather low velocity (<1 km/s) and hence, can't demagnetize any volume, while Z-model is not reliable near the TC edge and gives higher velocities. However, the ejecta blankets thickness near the edge is high and can demagnetize the crust by another, not shock-induced mechanism (i.e. overturn of the crust or change of the internal planetary heat flux).

## 6. Discussion: Magnetic Remanence Carriers, Magnetization Mechanisms, and Distribution of Magnetization With Depth

[13] Martian crustal magnetic anomalies are unusually large in amplitude [e.g., *Connerney et al.*, 1999; *Hood et al.*, 2005]. A maximum depth of anomaly sources is provided by the depth of the Curie isotherm $T_C$, the temperature above which magnetization in a given mineral becomes unstable. Possible remanence carriers at Mars, in order of efficiency of thermoremanent magnetization acquisition in the terrestrial field are [*Clark*, 1983, 1997]: single domain magnetite $Fe_3O_4$ with $T_C$ = 580°C; single domain pyrrhotite $Fe_{1-x}S$; x < 0.13 with $T_C$ = 320°C; and multidomain hematite $Fe_2O_3$ with $T_C$ = 670°C. Thermal history models predict temperature gradients in the early Mars highland crust of ~20°C/km [e.g., *Schubert et al.*, 1992; *Schumacher and Breuer*, 2004]. Therefore, the maximum depth to the Curie isotherm for the above minerals ranges from ~16 km for pyrrhotite to ~33 km for hematite. Depending on grain size, all of the above minerals are capable of providing magnetization intensities of the required magnitudes [*Kletetschka et al.*, 2003; *Rochette et al.*, 2005].

[14] Theoretical modeling of spatial power spectra of the Mars crustal field has suggested a mean source depth of ~50 km [*Voorhies et al.*, 2002]. However, the dependence of this result on model assumptions is continuing to be evaluated (C. Voorhies, personal communication, 2005). It had been suggested that minimum source region depths could be estimated based on minimum crater sizes for which impact demagnetization signatures are observed [*Nimmo and Gilmore*, 2001]. However, recent applications of this approach have yielded inconclusive results because of the required small sizes of the craters and limits on resolution of available magnetic anomaly maps [*Mohit and Arkani-Hamed*, 2004]. Recently, evidence has been advanced that Martian crustal magnetic anomalies may be concentrated at low paleolatitudes [*Hood et al.*, 2005]. Assuming that subsurface water was more abundant at low paleolatitudes for meteorological reasons, such a concentration would be consistent with models in which hydrothermal alteration of crustal rocks (e.g., serpentinization of olivine and pyroxene to produce magnetite; decomposition of siderite to produce magnetite; formation of sulfide deposits containing pyrrhotite) was involved in producing the observed strong magnetization [see also *Harrison and Grimm*, 2002; *Scott and Fuller*, 2004]. If so, then the maximum depth of crustal anomaly sources would be limited by the depth of penetration of subsurface water, which could be 10 to 20 km (K. Harrison, personal communication, 2005).

## 7. Conclusions

[15] Outside the transient cavity demagnetization by secondary impacts is at least comparable with demagneti-

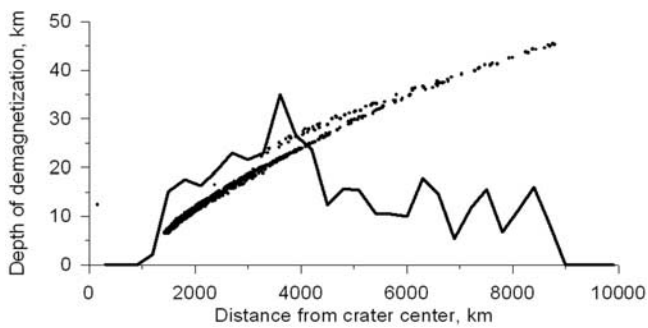


**Figure 4.** Demagnetization of the Martian crust along the line A-A′ in Figure 3 (see text for details).

zation in the direct shock wave. While the direct shock wave cannot demagnetize the uppermost layers of the crust because of its quick decay near the free surface, secondary impacts can demagnetize these same upper layers. The effect of SI-demagnetization strongly depends on the crater size and decreases sharply with the crater size decrease. It is negligible for basins smaller than ~500 km.

[16] Particular input from primary shock wave and secondary impacts depends on the magnetic carriers distribution in the crust: if magnetic minerals are mainly in the uppermost layers, then secondaries may be of a great importance. SI-demagnetization is substantially asymmetric in oblique impacts, while demagnetization by the impact itself is usually symmetric (only the highest pressure isobars near an impact site are asymmetric).

[17] **Acknowledgment.** This work was supported by a grant from the NASA Mars Data Analysis Program.

## References

Acuña, M., et al. (1999), Global distribution of crustal magnetization discovered by the Mars Global Surveyor MAG/ER experiment, *Science*, *284*, 790–793.

Amsden, A. A., H. M. Ruppel, and C. W. Hirt (1980), SALE, a simplified ALE computer program for fluid flow at all speeds, *Rep. LA-8095*, 101 pp., Los Alamos Natl. Lab., Los Alamos, N. M.

Artemieva, N., and B. Ivanov (2004), Launch of Martian meteorites in oblique impacts, *Icarus*, *171*, 84–101.

Clark, D. A. (1983), Comments on magnetic petrophysics, *Bull. Aust. Soc. Explor. Geophys.*, *14*, 40–62.

Clark, D. A. (1997), Magnetic petrophysics and magnetic petrology: Aids to geological interpretation of magnetic surveys, *J. Aust. Geol. Geophys.*, *17*(2), 83–103.

Connerney, J. E. P., M. Acuña, P. Wasilewski, N. Ness, H. Rème, C. Mazelle, D. Vignes, R. Lin, D. Mitchell, and P. Cloutier (1999), Magnetic lineations in the ancient crust of Mars, *Science*, *284*, 794–798.

Harrison, K. P., and R. E. Grimm (2002), Controls on Martian hydrothermal systems: Application to valley network and magnetic anomaly formation, *J. Geophys. Res.*, *107*(E5), 5025, doi:10.1029/2001JE001616.

Hauck, S. A., and R. J. Phillips (2002), Thermal and crustal evolution of Mars, *J. Geophys. Res.*, *107*(E7), 5052, doi:10.1029/2001JE001801.

Hood, L. L., N. C. Richmond, E. Pierazzo, and P. Rochette (2003), Distribution of crustal magnetic fields on Mars: Shock effects of basin-forming impacts, *Geophys. Res. Lett.*, *30*(6), 1281, doi:10.1029/2002GL016657.

Hood, L. L., C. Young, N. C. Richmond, and K. Harrison (2005), Modeling of major Martian magnetic anomalies: Further evidence for polar reorientations during the Noachian, *Icarus*, *177*, 144–173.

Ivanov, B. A. (2003), Complex crater formation: Verification of numerical models, paper presented at Impact Cratering: Bridging the Gap Between Modeling and Observations, Lunar and Planet. Inst., Houston, Tex.

Ivanov, B. A., and L. I. Comissarova (1977), The simple hydrodynamic model of cratering, *Lunar Planet. Sci. Conf.*, *VIII*, 499–501.

Kletetschka, G., N. F. Ness, P. J. Wasilewski, J. E. P. Connerney, and M. H. Acuna (2003), Possible mineral sources of magnetic anomalies on Mars, *Leading Edge*, *22*, 766–768.

Maxwell, D. E. (1977), Simple Z model of cratering, ejection, and the overturned flap, in *Impact and Explosion Cratering*, edited by D. J. Roddy et al., pp. 1003–1008, Elsevier, New York.

Mohit, P. S., and J. Arkani-Hamed (2004), Impact demagnetization of the Martian crust, *Icarus*, *168*, 305–317.

Moore, H. J. (1971), Large blocks around lunar craters, in *Analysis of Apollo 10 Photography and Visual Observations*, *NASA Spec. Publ.*, *NASA-SP 232*, 26–27.

Nimmo, F., and M. S. Gilmore (2001), Constraints on the depth of magnetized crust on Mars from impact craters, *J. Geophys. Res.*, *106*(E6), 12,315–12,323.

Rochette, P., J. Gattacceca, V. Chevrier, V. Hoffmann, J. P. Lorand, M. Funaki, and R. Hochleitner (2005), Matching Martian crustal magnetization and meteorite magnetic properties, *Meteorit. Planet. Sci.*, *40*, 529–540.

Schmidt, R. M., and K. R. Housen (1987), Some recent advances in the scaling of impact and explosion cratering, *Int. J. Impact Eng.*, *5*, 543–560.

Schubert, G., S. C. Solomon, D. L. Turcotte, M. J. Drake, and N. H. Sleep (1992), Origin and thermal evolution of Mars, in *Mars*, edited by H. H. Kieffer et al., pp. 147–183, Univ. of Ariz. Press, Tucson.

Schumacher, S., and D. Breuer (2004), Effects of thermal conductivity of crust and lithosphere on the temperature evolution of Mars, *Geophys. Res. Abstr.*, *6*, Abstract EGU04-A-03653.

Scott, E. R. D., and M. Fuller (2004), A possible source for the Martian crustal magnetic field, *Earth Planet Sci. Lett.*, *220*, 83–90.

Shuvalov, V. V. (1999), Multidimensional hydrodynamic code SOVA for interfacial flows: Application to the thermal layer effect, *Shock Waves*, *9*, 381–390.

Steel, D. (1998), Distributions and moments of asteroid and comet impact speeds upon the Earth and Mars, *Planet. Space Sci.*, *46*, 473–478.

Thompson, S. L., and H. S. Lauson (1972), Improvements in the Chart D radiation-hydrodynamic CODE III: Revised analytic equations of state, *Rep. SC-RR-71 0714*, 119 pp., Sandia Natl. Lab., Albuquerque, N. M.

Vickery, A. M. (1986), Size-velocity distribution of large ejecta fragments, *Icarus*, *67*, 224–236.

Voorhies, C. V., T. J. Sabaka, and M. Purucker (2002), On magnetic spectra of Earth and Mars, *J. Geophys. Res.*, *107*(E6), 5034, doi:10.1029/2001JE001534.

N. Artemieva and B. A. Ivanov, Institute for Dynamics of Geospheres, Leninsky Prospect 38, Building 1, 119334 Moscow, Russia. (artemeva@psi.edu; ivanov@idg.chph.ras.ru)

L. Hood, Lunar and Planetary Laboratory, University of Arizona, 1629 East University Boulevard, Tucson, AZ 85721-0092, USA. (lhood@lpl.arizona.edu)